Seismic Risk Analysis of Regular Girder Bridge Subjected to Mainshock-Aftershock Sequences

LIBO CHEN (lbchen@fzu.edu.cn)
Fuzhou University https://orcid.org/0000-0003-4685-6421
Jianhong Zhou
Fuzhou University
Qiluan Zhou
Fuzhou University

Research Article

Keywords: mainshock-aftershock sequence, seismic hazard, aftershock fragility, damage transition probability matrix, seismic risk

Posted Date: December 6th, 2021

DOI: https://doi.org/10.21203/rs.3.rs-1122449/v1

Seismic Risk Analysis of Regular Girder Bridge Subjected to Mainshock-Aftershock Sequences

Libo Chen[1]; Jianhong Zhou[1]; Qiluan Zhou[1]
[1]College of Civil Engineering,Fuzhou University, Fuzhou, China.
Affiliation: Libo Chen: lbchen@fzu.edu.cn

Abstract: When a structure is subjected to an earthquake sequence, the high rate of aftershocks after the mainshock and cumulative damage caused by the earthquake sequence make the structure very dangerous. Considering the uncertainty in seismic occurrences, structural damage is often predicted using a seismic risk analysis. This approach has become a main measure for seismic disaster assessment, and provides a reasonable reference for post-earthquake emergency response decision-making and pre-earthquake seismic design. Therefore, it is of great significance to study a seismic risk analysis considering the effect(s) of aftershocks. In this study, the aftershock hazard is estimated for a post-mainshock environment based on an aftershock probabilistic seismic hazard analysis. Considering the uncertainty regarding the mainshock and aftershock occurrences, in addition to the functional relationship between the mainshock and aftershock parameters, the aftershock seismic hazard is estimated for the pre-mainshock environment. The mainshock fragility and aftershock fragility of regular girder bridges are evaluated based on the Kunnath damage model. Finally, considering the damage accumulation in bridge structures, the seismic hazard and seismic fragility are combined to establish a post-mainshock aftershock seismic risk framework and pre-mainshock mainshock-aftershock seismic risk analysis framework. Based on these, the mainshock risk and mainshock-aftershock risk are compared to verify the importance of considering the aftershock effects in seismic disaster assessments. The aftershock risks for the bridges of different post-mainshock damage states are compared, and the influence of the initial damage after the mainshock on the damage to the structure in the post-mainshock environment is studied.

Key words: mainshock-aftershock sequence; seismic hazard; aftershock fragility; damage transition probability matrix; seismic risk

1 Introduction

Bridge structures are highly susceptible to damage during seismic events, potentially resulting in substantial property damage and human casualties. Earthquakes often occur in the form of earthquake sequences, and the cumulative effect of the high-rate aftershocks and damage caused from these sequential earthquakes after the main earthquake causes these structures to remain very dangerous in the aftershock environment. Considering the uncertainty in seismic performances

and seismic occurrences, seismic structural damage is often predicted via a seismic risk analysis. This approach has also become the main measure in seismic disaster assessment (Moehle and Deierlein 2004). Therefore, there is great significance in providing a seismic risk analysis able to consider the effects of aftershocks.

The occurrence rate of an aftershock peaks immediately after the mainshock, and decreases with time (Yeo and Cornell 2009). Reasenberg and Jones (Reasenberg and Jones 1989) developed a statistical model for predicting aftershock occurrence based on a non-homogenous Poisson process, and used point estimates for constant model parameters to predict the probability of earthquake occurrence. Yeo and Cornell (Yeo and Cornell 2009) also used a non-homogenous Poisson process to characterize aftershocks, and proposed the aftershock probabilistic seismic hazard analysis (APSHA) by adopting the product of the mean aftershock rate and probability distribution of the aftershock intensity as the result of the seismic hazard during the research period. This analysis focused on the effects on the structure from the aftershock. Ebrahimian et al. (Ebrahimian et al. 2014) improved the accuracy of aftershock hazard parameters using a Bayesian-based approach. Iervolino et al. (Iervolino et al. 2014) evaluated the seismic hazards of an earthquake cluster; they considered that the cluster had the same return period as the mainshock (Toro and Silva 2001; Boyd 2012), and evaluated the seismic hazard of the cluster while considering the uncertainties in both the mainshock and aftershock. The above studies verify the rationality of conducting a pre-mainshock assessment for aftershock hazards.

As an important part of a seismic risk analysis, the "seismic vulnerability" refers to the probability of exceeding the limit state of a structure subjected to a specific intensity of ground motion. In fact, the damage exceedance probability of a structure subjected to a mainshock-aftershock sequence is significantly higher than that to a mainshock, as aftershocks will cause additional damage. The expressions for the mainshock-aftershock fragility are different, including the state-dependent vulnerability curve (Ryu et al. 2011; Zhang el al. 2020), intensities-dependent vulnerability curve (Fu 2015), and event-dependent aftershock vulnerability curve (Ebrahimian et al. 2014).

Ryu et al. (Ryu et al. 2011) obtained the seismic response under a mainshock-aftershock sequence using an incremental dynamic analysis method, and generated a state-dependent collapse fragility curve for a mainshock-damaged frame while considering the uncertainty in the damage state limits. Zhang et al. (Zhang el al. 2020) considered the amplitudes of seismic sequence records with moderate scaling factors as the earthquake input, and then calculated the seismic response and damage transition probability of a timber frame structure. Fu (Fu 2015) proposed a probabilistic seismic demand model under a mainshock-aftershock sequence, and obtained the relationship between the structural damage probability and the intensities of both the mainshock

and aftershock. A double multiple stripe analysis (double-MSA) was adopted to obtain a sufficient number of response samples, in which the intensities of the mainshock and aftershock were scaled to a predetermined level to enrich the inputs of the ground motions. Ebrahimian et al. (Ebrahimian et al. 2014) obtained the relationship between the structural damage probability and number of aftershocks by randomly connecting multiple aftershocks from the same sequence to obtain a number of samples. In general, an intensity-dependent fragility is only applicable to a mainshock–aftershock pair. In contrast, the accuracy of an event-dependent vulnerability is more sensitive to the universality of ground motion characteristics and number of selected ground motions. However, with an increase in the number of aftershocks, the required amount of calculations increase significantly. A state-dependent vulnerability can directly describe the seismic capacity of damaged structures with a relatively small number of calculations. Consequently, it is currently widely used.

A post-mainshock–aftershock risk assessment is applicable to the prediction of structural damage in aftershock environments after the occurrence of the mainshock. It provides a theoretical reference to help decision-makers master the operations of a traffic bridge system in the disaster area from a probability perspective, and to determine the priorities of bridge reinforcements. Ebrahimian et al. (Ebrahimian et al. 2014) comprehensively considered the uncertainties in the aftershock intensity and number of aftershocks and an event-dependent vulnerability function to obtain the daily damage probability of a structure. Alessandri et al. (Alessandri et al. 2013) combined a vulnerability model based on an incremental dynamic analysis with an APSHA to estimate the mean annual damage rate of a structure. Although experimental observation data were introduced to update the seismic vulnerability, the procedure for obtaining the annual average damage rate failed to consider the damage accumulation of the bridge structure during multiple aftershocks.

A pre-mainshock mainshock-aftershock risk assessment framework can be established based on the consideration of the uncertainty in the mainshock and aftershock occurrences. It is suitable for assessing an earthquake swarm disaster before the occurrence of the mainshock. By predicting the damage of the structure when subjected to a future earthquake swarm, it provides a theoretical reference for seismic fortification before the mainshock. Simultaneously, it also provides a new approach to improving the current seismic design standard (which only considers the mainshock condition), and optimizes the seismic design scheme to make the structure capable of withstanding the earthquake swarm. Jalayer et al. (Jalayer et al. 2017) simplified the mainshock parameters to a uniform distribution and combined an event-dependent vulnerability function curve with Omori's law to obtain a daily damage state exceeding a probability. However, its simplified consideration of the uncertainty in the occurrence of mainshocks led to low reliability in the prediction results.

Veismoradi et al. (Veismoradi et al. 2018) calculated the annual collapse probability of a structure under the effects of a mainshock and aftershock based on a total probability formula, i.e., by integrating the conditional collapse probability of the structure in all possible damage states after the mainshock. However, the model failed to consider damage accumulation during the damage process, and the results could not reflect the time-varying law of the structural damage.

Accordingly, to predict the bridge damage when a bridge subjected to the mainshock and aftershock, a mainshock risk model and aftershock risk model are respectively established, in this study, as discussed in Section 2. Based on the APSHA method, the aftershock hazard curve for a specific mainshock and mainshock-aftershock hazard curve are obtained, in consideration of the uncertainty in the mainshock parameters. A finite element model of the bridge is established using OpenSees, as discussed in Section 3. The scaled real mainshock and aftershock records are input into the finite element model of the bridge to obtain the seismic response. The mainshock vulnerability and aftershock vulnerability of the bridge are evaluated based on the Kunnath damage model. As discussed in Section 4, considering the damage accumulation from earthquakes, the seismic vulnerability and seismic hazard are combined to establish a (1) post-mainshock aftershock risk assessment framework and (2) pre-mainshock mainshock-aftershock risk assessment framework. Through comparative analysis, the influence of aftershocks on the seismic risk and of the post-mainshock damage state on the aftershock risk are elaborated on.

2 Probabilistic mainshock-aftershock seismic hazard analysis

2.1 Probabilistic mainshock seismic hazard analysis model

A ground motion intensity can directly describe the impact of an earthquake on a structure at a research site. A solution to a ground motion intensity problem is not only helpful for grasping the situation of an earthquake, but can also be used for the prediction of structural damage (which is of great significance). The specific steps are as follows: a) determine the fault and seismic parameters, such as the upper limit of magnitude, lower limit of magnitude, and distribution parameter of the magnitude b; b) determine the probability density function of the magnitude based on the relationship between the magnitude and frequency (Gutenberg et al. 1944); and c) determine the probability density function of the source-to-site distance according to the relative positional relationship between the site and fault rupture. When the length of the earthquake rupture is unknown, it can be calculated using an empirical formula (Wells et al. 1994). The rupture is assumed to extend symmetrically from the epicenter to both sides (Kiureghian et al. 1977). The location is assumed to be uniformly distributed. As an additional step, the process further comprises d) integrating the magnitude distribution function, source site distance distribution function, and conditional intensity exceedance probability given by the ground motion prediction

equations (Boore et al. 2008) to calculate the ground motion intensity exceedance probability, as shown in Eq. (1).

$$\begin{aligned} P(IM > x) &= \int_R \int_{m_{\min}}^{m_{\max}} P(IM > x \mid m, r) f_{R|M}(r \mid m) f_M(m) \mathrm{d}m \mathrm{d}r \\ &\approx \sum_M \{P(M = m_i) \sum_R [P(IM > x \mid m_i, r_j) P(R = r_j \mid m_i)]\} \end{aligned} \tag{1}$$

In the above, $f_M(m)$ denotes the probability density function for M; $f_{R|M}(r \mid m)$ denotes the probability density function of the source-to-site distance for the specific mainshock with a magnitude of m; and $P(IM > x \mid m, r)$ can be obtained through ground motion prediction equations.

By introducing the mean annual rate of the research fault, the exceedance rate of the ground motion intensity of the research site can be further calculated according to Eq. (2).

$$\begin{aligned} \lambda(IM > x) &= \lambda(M > m_{\min}) \int_R \int_{m_{\min}}^{m_{\max}} P(IM > x \mid m, r) f_{R|M}(r \mid m) f_M(m) \mathrm{d}m \mathrm{d}r \\ &\approx \lambda(M > m_{\min}) \sum_M \{P(M = m_i) \sum_R [P(IM > x \mid m_i, r_j) P(R = r_j \mid m_i)]\} \end{aligned} \tag{2}$$

Here, $\lambda(M > m_{\min})$ denotes the mean annual rate of an earthquake with a magnitude larger than $m_{\min}$. It can be determined through an analysis of seismicity trends.

2.2 Aftershock probabilistic seismic hazard analysis model

2.2.1 Mean number of aftershocks

The rate of occurrence of aftershocks is not constant, with the peak value immediately following the mainshock, followed by decreasing with increasing elapsed time from the occurrence of the mainshock. The modified Omor's law is still the most widely used method for describing the average occurrence rate of aftershocks. Yeo and Cornell (Yeo and Cornell 2009) derived the daily average occurrence rate of aftershocks based on a modified Omor's Law (Utsu et al. 1995) and the magnitude-frequency relationship (Gutenberg et al. 1944), as follows:

$$v(t) = \mu(t; m_{\mathrm{m}}) = \frac{10^{a+b(m_{\mathrm{m}}-m_{\mathrm{l}})} - 10^{a}}{(t+c)^{p}} \tag{3}$$

In the above, m_{l} is the lower limit of the aftershock magnitude, and $\mu(t; m_{\mathrm{m}})$ denotes the mean daily rate density of aftershocks with magnitudes between m_{l} and m_{m} at time t following a mainshock of magnitude m_{m}. The mean number of aftershocks with magnitudes between m_{l} and m_{m} in the time interval $[t, t+T]$ following a mainshock of magnitude m_{m} (denoted as $\mu(t, T; m_{\mathrm{m}})$) can be calculated as follows:

$$\mu(t, T; m_{\mathrm{m}}) = \int_t^{t+T} \mu(\tau; m_{\mathrm{m}}) \mathrm{d}\tau = \frac{10^{a+b(m_{\mathrm{m}}-m_{\mathrm{l}})} - 10^{a}}{p-1} [(t+c)^{1-p} - (t+T+c)^{1-p}] \tag{4}$$

Similar to the traditional probabilistic seismic hazard analysis (PSHA), the exceedance

probability of the aftershock intensity can be obtained as follows. First, the magnitude-frequency relationship is adopted, where the lower limit of the magnitude is the same as the lower limit of the mainshock, and the upper limit of magnitude is the mainshock magnitude (Yeo and Cornell 2009). Second, it is assumed that the aftershock epicenter location is uniformly distributed within only the mainshock rupture, and that the aftershock rupture extends symmetrically to both sides along the mainshock fault direction (Kiureghian et al. 1977). In addition, its length is obtained by an empirical formula. Third, based on the full probability formula, the exceedance probability for all possible aftershock magnitudes and source-to-site distance conditions are integrated.

$$P(IM > x) = \int_R \int_{m_l}^{m_m} P(IM > x \mid m, r) f_{R|M}(r \mid m) f_M(m; m_m) \mathrm{d}m\mathrm{d}r \tag{5}$$

Here, $f_M(m; m_m)$ is the probability density function of the aftershock magnitude for a given mainshock with a magnitude of m_m, and $f_{R|M}(r \mid m)$ is the probability density function of the aftershock source-to-site distance. The mean number of aftershocks exceeding a specific seismic intensity within a specific time interval is expressed as the product of the mean number of aftershocks and the probability of exceeding the ground motion intensity, as shown in Eq. (6).

$$\mu(x, t, T; m_m) = \mu(t, T; m_m) \int_R \int_{m_l}^{m_m} P(IM > x \mid m, r) f_{R|M}(r \mid m) f_M(m; m_m) \mathrm{d}m\mathrm{d}r \tag{6}$$

In the above, $\mu(x, t, T; m_m)$ is the mean number of aftershocks exceeding a site ground motion y within the time interval [t, t+T] following a mainshock of magnitude m_m.

2.2.2 Aftershock parameters

The aftershock parameters determine the mean number of aftershocks, including a, c, and p, and are usually estimated according to a historical earthquake catalogue. Page et al. [20] proposed a procedure for estimating aftershock parameters based on the Reasenberg and Jones model (Reasenberg and Jones 1989) and a newly proposed time-varying magnitude completeness function. Aftershock parameters are different in different regions, e.g., according to the global seismotectonic zoning map proposed by Garcia et al. (Garcia et al. 2012). The generic parameters for the different regions are determined by using a worldwide earthquake catalogue; these can be used as the aftershock parameters for a pre-mainshock analysis for an unknown aftershock catalogue. When the catalogue of aftershocks is collected after the mainshock, the updated aftershock parameters (updated based on a Bayesian law) can increase the accuracy of the aftershock prediction. However, the research shows that the estimation results for all parameters updated simultaneously are not stable. Thus, the parameters c and p of the aftershock prediction remain constant for a long time after the main earthquake, and Bayesian updating is only carried out for the parameter a (Page et al. 2016) . A Bayesian update is conducted based on the likelihood function formula proposed by Ogata (Ogata 1983) to determine the influence of the aftershock catalogue on the parameter distribution.

$$\ln L = \sum_i \ln\lambda(t_i, M_c(t_i)) - \int_{t_0}^{t_1} \lambda(t, M_c(t))\mathrm{d}t \tag{7}$$

Here, t_0 is the moment of occurrence of the mainshock. t_1 is the end moment of the observed catalogue. t_i is a different moment when a different aftershock occurs.

$$\lambda(t, m_1) = 10^{a+b(m_m - m_1)} \cdot (t+c)^{-p} \tag{8}$$

The generic distribution of the parameter is adopted as the prior distribution. The posterior distribution is obtained as follows (Michael et al. 2019):

$$\mathrm{PDF}_{\mathrm{Bayes}}(a) = \frac{\mathrm{PDF}_{\mathrm{generic}}(a)L(a)}{\sum_j \mathrm{PDF}_{\mathrm{generic}}(a_j)L(a_j)} \tag{9}$$

In the above, a_j are discretized values. The United States Geological Survey recommends a value range of [- 4.5, - 0.5] to ensure that 99.73% of the values are considered.

2.3 Mainshock seismic hazard analysis

In 2008, the Wenchuan Earthquake occurred in Wenchuan, Sichuan Province, causing a large number of casualties and structural damage. Wenchuan is close to the Longmenshan fault, which has high seismicity. Therefore, this section considered Guxigou Bridge in Wenchuan County as the site for conducting the mainshock risk analysis. In this study, the Longmenshan Central Fault was taken as an example fault to predict future earthquakes. This fault passes through Yingxiu, Beichuan, and so on, and is a reverse strike slip fault. In this study, the fault was simulated by a line source with a length of approximately 486 km and a strike of N 45°E. Because there were earthquakes with magnitudes of 8.0 in the Longmenshan Fault, the upper limit of the magnitude is 8.0, and considering that earthquakes with magnitudes less than 5.0 have little influence on a structure, the lower limit of the magnitude was 5.0. The parameter b from the magnitude-frequency relationship was 0.728, according to the division scheme of the seismic zones in the original zoning map. Spectral acceleration was selected as the ground motion intensity index. The mainshock seismic hazard curve is shown in Fig. 2.

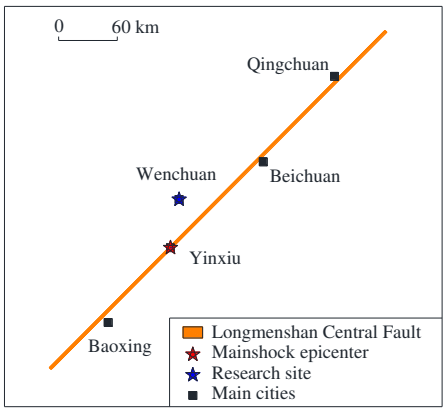

Fig. 1 Location of the site and the fault

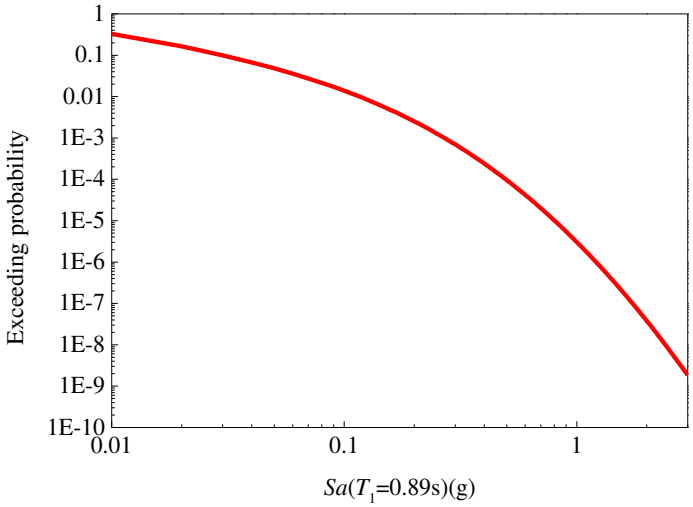

Fig. 2 Mainshock intensity exceedance probability curve

Fig. 2 shows the exceedance probability of ground motion intensity for the site as caused by the earthquake of the Longmenshan Central Fault. It can be seen from the figure that the exceedance probability of ground motion intensity decreases with an increase of the ground motion intensity. The decrease is faster when the spectral acceleration is smaller, and becomes slower as the spectral acceleration increases.

2.4 Aftershock probabilistic seismic hazard analysis

As discussed in this section, based on the APSHA approach, we first considered the Wenchuan earthquake as an example to analyze the post-mainshock aftershock seismic hazard. Then, considering the uncertainty of the mainshock parameters, the Longmenshan Central Fault was taken as an example to analyze the pre-mainshock mainshock–aftershock seismic hazard. The generic parameters were determined according to the location of Wenchuan as $a_{\text{mean}} = -2.13$ $a_{\sigma} = 0.52$. The parameters satisfied a normal distribution with $c = 0.018$, $p = 0.98$, and $b = 1.0$. Based on the catalogue of aftershocks from within 3 days after the mainshock, Bayesian updating was performed, and the updated parameters were $a = \text{-}1.852$, $c = 0.018$, $p = 0.98$, and $b = 1.0$.

2.4.1 Aftershock seismic hazard curve for specific mainshock

The purpose of this study was to analyze the time-varying seismic damage exceedance probability of the bridge structure. In general, considering that an aftershock hazard declines after the mainshock, it is commonly at a low level 30 days after the mainshock. Moreover, reinforcement measures may be installed within this 30 days. As such, it is not necessary to analyze the seismic risk once 30 days have passed after the mainshock. Therefore, this study assumed a period of 30 days for the research period of aftershock seismic risk, and that the structure was repaired after 30 days. The research period was divided into sections according to a time step of 0.0005 days. The exceedance rate of the aftershock intensity in each time window was calculated.

$$\lambda_{IM}^{t_0,t_1}(IM>x)=v^{AS}[t_0,t_1]\cdot \sum_{M^{AS}}\{P(M^{AS}=m_i;m_{\mathrm{m}})\sum_{R^{AS}}[P(IM>x\,|\,m_i,r_j)P(R=r_j\,|\,m_i)]\} \tag{10}$$

In the above, $v^{AS}[t_0,t_1]$ is the mean number of aftershocks in the time interval $[t_0,t_1]$. The upper limit of the magnitude is 7.9, and the lower limit of the magnitude is 5.0. According to the empirical formula, the rupture length of the mainshock is 131 km $V_{S30}=519$ m/s. The exceedance rate of aftershock intensity is shown in Fig. 3.

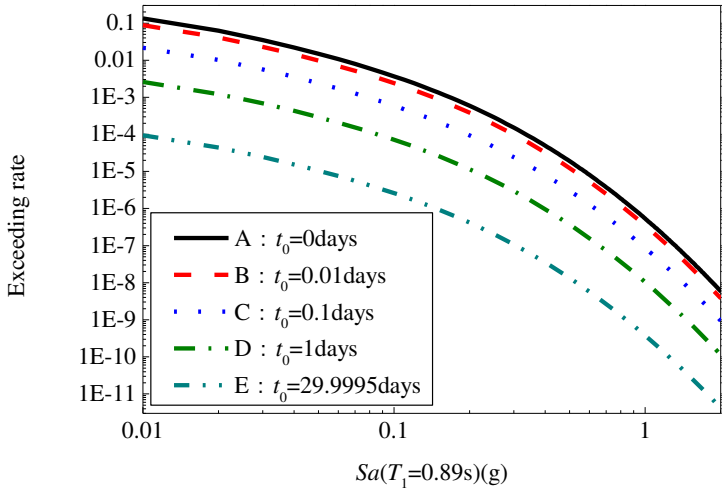

Fig. 1 Aftershock intensity exceedance rate curve for specific mainshocks

The five aftershock hazard curves in Fig. 3 correspond to five star points of the research time window with a length of 0.0005 days. The aftershock hazard is higher than that of the mainshock, verifying the necessity of considering the influences of aftershocks on a structure. The curves are basically parallel (when the ordinates are logarithmic coordinates, the parallel lines indicate that that the ratio of the values for every spectral acceleration is always equal). This is because the APSHA assumes that the intensity exceedance probabilities of aftershocks occurring at different times as triggered by the same mainshock are independent of each other, and meet the same distribution. The differences in the ordinates of the five curves are owing to the differences in the mean aftershock number in the different time windows, and reflect that the aftershock occurrence rate decreases with time.

2.4.2 Mainshock-aftershock seismic hazard curve

There are many uncertain factors in the occurrence of a mainshock, but the most important factors affecting the aftershock hazard are the magnitude and epicenter location of the mainshock. Therefore, a prediction of the aftershock hazard when the mainshock information is unknown can be conducted by combining the PSHA and APSHA to comprehensively consider the uncertainty of the mainshock and aftershock occurrences. This section considers the Longmenshan Central Fault as an example.

In the APSHA, the mean number of aftershocks and upper limit of the aftershock distribution

are determined based on the magnitude of the mainshock. The possible location of the aftershocks is determined based on the magnitude of the mainshock and the location of the epicenter. The procedure for obtaining the aftershock hazard while considering the uncertainty of the mainshock parameters is as follows: a) the uncertainty of the mainshock magnitude is considered according to the PSHA method; b) the epicenter of the mainshock is assumed to have a uniform distribution at any position on the fault line source, an considering each combination of magnitude and epicenter location of the mainshock as the known condition, using generic aftershock parameters in the Wenchuan area, the procedure of the APSHA is repeated; and c) the product of the probability of each group of possible magnitude and epicenter and the corresponding exceedance rate of the aftershock ground motion intensity is accumulated with the full probability formula to obtain the overall exceedance rate of the aftershock ground motion intensity. The calculation process is given by Eq. (11), and the aftershock hazard results before the mainshock are shown in the figure below.

$$\begin{aligned}\lambda(IM > x) &= \sum_{M^{MS}} P(M_i^{MS})\lambda(M_i^{MS})P(IM > x|M_i^{MS}) \\ &= \sum_{M^{MS}} \left\{ P(M_i^{MS})\lambda(M_i^{MS}) \sum_{X^{MS}} [P(IM > x \,|\, M_i^{MS}, X_j^{MS})P(X_j^{MS})] \right\}\end{aligned} \tag{11}$$

Here, M^{MS} is the mainshock magnitude; $\lambda(M_i^{MS})$ is the mean number of aftershocks triggered by the mainshock with a magnitude of M_i^{MS} in a specific time interval; X^{MS} is the Variable of the mainshock epicenter; and X_j^{MS} denotes the linear distance between the possible location of the mainshock epicenter and the left end of the fault.

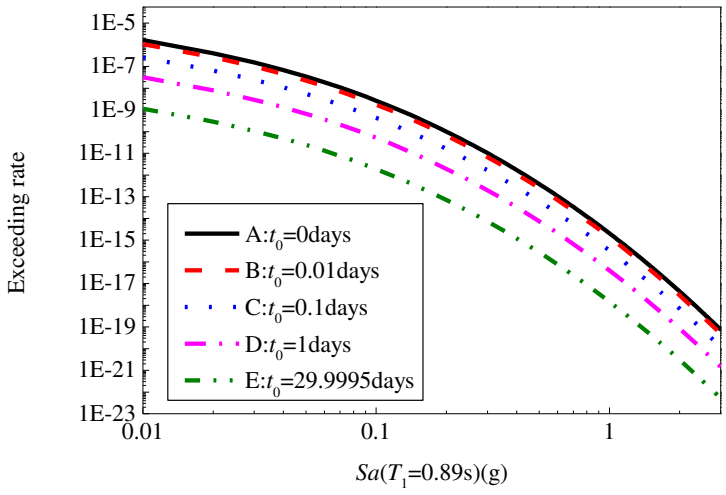

Fig. 2 Aftershock intensity exceedance rate considering the uncertainty of mainshock

The curves in Fig. 4 show the aftershock ground motion intensity exceedance rate function considering the uncertainty of the occurrence of the mainshock. The duration of the study time window is 0.0005 days. It can be seen from the figure that the aftershock occurrence rate with an earlier starting time is always above that with a later starting time. The five curves in the figure

are basically parallel, indicating that in the pre-mainshock seismic hazard analysis considering the uncertainty of the mainshock parameters, the main factor causing the differences in the aftershock intensity exceedance rates is the mean number of aftershocks. Comparing the curve in Fig. 4 with that in Fig. 3, the hazard from the aftershock predicted before the mainshock is smaller. This is because although a strong mainshock can trigger aftershocks with a higher occurrence rate, the low probability of a strong mainshock weakens the contribution of the aftershock occurrence rate. The aftershock hazard for a small mainshock with a higher occurrence probability is relatively lower.

3 Mainshock-aftershock seismic fragility analysis for regular bridge

3.1 Case bridge

In this study, the Guxigou bridge was taken as an example to analyze the seismic vulnerability of regular girder bridges while considering the effect of the mainshock-aftershock sequence. It is a three-span prestressed concrete simply supported girder bridge. Each span of the bridge is 30 m. The superstructure comprises four T-beams. The height of the main beam is 2 m, and the bridge deck width is 8 m. The capbeam section is rectangular, with a length of 8 m. There is a double-column concrete pier with a spacing of 4.8 m, and the section is a circle with a diameter of 1.5 m. The thickness of the concrete cover is 0.06 m. In addition, 26 longitudinal reinforcements each with a diameter of 25 mm are evenly distributed on the circumference. Spiral stirrups are arranged along the full length of the pier, and the distance between them is 0.15 m. The foundation is a pile foundation with a diameter of 1.8 m, spacing of 4.8 m, and length of 20 m. According to the Chinese code for the seismic design of highway bridges (Ministry of Transport 2020), this bridge is a regular beam bridge. In this study, the numerical simulation of the bridge example in this section was performed using OpenSees software (Mazzoni et al. 2006).

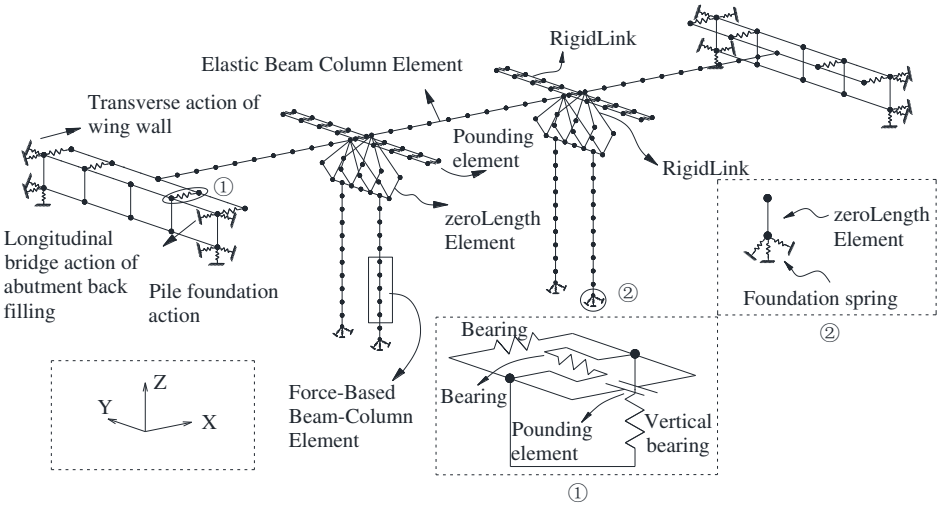

Fig. 5 Finite element model of bridge

In particular, elastic beam column elements were adopted to model the beam, and a force-based beam column element was used to model the substructure. The "Concrete02" material was selected to simulate the constitutive relationship of the concrete in the substructure. A hysteretic material was selected to simulate the effect of the steel reinforcement used in the substructure. In the finite element simulation of the abutment, a hyperbolic gap material was selected to simulate the constraining effect of the passive earth pressure produced by the backfill after pounding on the longitudinal displacement of the abutment. Moreover, a hysteretic material was selected to describe the restriction of the pile foundation on the longitudinal displacement of the abutment. Rigid arm and zero-length elements were used to connect the abutment and main beam as a whole to adequately describe the stiffness of the abutment. A bilinear model was selected for the simulation of the plate rubber bearing (Ye et al. 2001).

3.2 Damage model

In general, to quantify structural damage according to the different damage mechanisms of bridge structures under earthquakes, scholars have established damage models based on specific performance indexes of bridge structures during earthquakes, including single-parameter and double-parameter types. A double-parameter model uses a deformation-energy-related composite index to describe the damage to the structure. Because it can comprehensively reflect the combined effect of cyclic loading and the damage caused by large displacements, the double-parameter damage model has additional advantages when considering the effects of seismic sequences. The commonly used double-parameter models mainly include the Park Ang damage model (Park et al. 1985), Kunnath damage model (Kunnath et al. 1990), and Kumar model (Kumar and Usami 1996). Kunnath (Kunnath et al. 1990) used a yield curvature to modify the displacement term. In this study, the Kunnath damage model was selected, and its specific model formula is shown in Eq. (12).

$$D = \frac{\varphi_m - \varphi_y}{\varphi_u - \varphi_y} + \beta \frac{E}{M_y \varphi_y} \tag{12}$$

In the above, the first term represents the deformation contribution; the second term represents the hysteretic energy contribution; φ_m is the curvature limit under the loading of the ground motion; φ_u is the ultimate failure curvature under monotonic loading; and φ_y is the yield curvature. M_y denotes the yield moment, and reflects the contribution of the hysteretic energy consumption to the damage index. The value generally depends on the size, reinforcement, and axial force of the component, and can be calculated as follows:

$$\beta = (-0.447 + 0.073 l / d + 0.24 n_0 + 0.314 \rho_t) \times 0.7^{\rho_w} \tag{13}$$

Here, ρ_w represents the stirrup ratio of the component volume; l/d is the shear-span ratio; n_0 represents the axial-compression ratio of the component; and ρ_t represents the longitudinal reinforcement ratio of the member. According to the information of the bridge, XTRACT is used to conduct the moment-curvature analysis of the pier section (Chadwell and Imbsen 2004), where $\varphi_y = 2.20\text{E}-03$, $\varphi_u = 2.07\text{E}-02$, M_y=3.44E+06N·m, and $\beta = 1.40\text{E}-01$.

Based on the Kunnath damage model, Stone and Taylor (Stone and Taylor 1993) proposed a four-level performance classification model based on a large amount of experimental data for circular section piers, as shown in the table below.

Table 1 Kunnath four-level performance classification model

Performance Level	Damage Index	Damage State	*DS*
Level I	$DI < 0.11$	Intact	1
Level II	$0.11 \le DI < 0.4$	Repairable	2
Level III	$0.4 \le DI < 0.77$	Unrepairable	3
Level IV	$DI \ge 0.77$	Collapse	4

3.3 Double-multiple stripe analysis (MSA)

Next, 61 mainshock and aftershock records were selected from the Pacific Earthquake Engineering Research Center-Next Generation Attenuation database, and the records were modified and truncated to ensure the accuracy of the calculations while reducing the amount of calculations required. The mainshock and aftershock were connected in series, and a free vibration interval of 20 s was inserted between them.

To obtain sufficient mainshock and aftershock response samples, Zhang et al. (Zhang et al. 2020) identified an appropriate overall equal scale for real mainshock and aftershock sequences. Wen et al. (Wen et al. 2017) limited the scaled intensity of a mainshock to within the scope of a bridge collapse, and scaled the corresponding aftershocks according to the intensity ratio IM_{AS}/IM_{MS}. In this study, the 61 selected mainshocks and aftershocks were used for a double MSA. First, each mainshock was scaled to generate a series of ground motions with increasing strength as the input for the finite element analysis. The structural response under each level of ground motion intensity was obtained through a nonlinear dynamic time history analysis. Second, scaled aftershocks with different intensities were applied to the damaged bridge structure after the mainshock to obtain the sequence response samples of the structure. The specific double-MSA scheme was as follows.

The intensity of the mainshock was set from 0.1 g to 1.3 g in steps of 0.1 g. The ratio Sa_{AS}/Sa_{MS} was set as 0.1, 0.2, 0.3, 0.4, 0.5, 0.6, 0.7, 0.8, and 1.0, respectively. The intensity of the aftershock was determined according to the ratio. The number of samples was $61\times13\times8 = 6344$.

3.4 Mainshock seismic fragility analysis

The fundamental period of the bridge was 0.89 s. The spectral acceleration at the fundamental period was selected as the ground motion intensity index. A lognormal distribution was used to fit the seismic fragility curves.

$$P(LS_{MS} \geq j \mid IM_{MS} = im) = \Phi\left[\frac{\ln(IM_{MS}) - \ln(\theta_{MS})}{\sigma_{MS}}\right] \tag{14}$$

Here, LS_{MS} denotes the post-mainshock limit state; IM_{MS} denotes the mainshock ground motion intensity; θ_{MS} and σ_{MS} denote the median and logarithmic standard deviation, respectively.

After obtaining the samples, a method based on an engineering demand parameter (EDP) criterion was used to estimate the two parameters of the above seismic vulnerability function.

$$P(DI_{MS} \geq DI_c \mid IM_{MS}) = \frac{\sum_{j=1}^{N} F_j}{N} \tag{15}$$

In the above, DI_{MS} is the damage index of the structure after the mainshock, DI_c represents a limit state value based on the Kunnath damage model, and F_j is the limit state function. N is the total number of response samples corresponding to the same seismic intensity level. According to the seismic response results from the MSA for a single mainshock, the frequency values of the intact structure beyond the limit value of each damage state can be obtained for different intensities of mainshock ground motions. In this study, the statistical parameters of the seismic vulnerability function were obtained based on the least square method.

Table 2 Bridge fragility function parameters

Repairable		Unrepairable		Collapse	
Median	Logarithmic standard deviation	Median	Logarithmic standard deviation	Median	Logarithmic standard deviation
0.880	0.255	1.073	0.270	1.229	0.255

As shown in the table, the median value of the ground motion intensity corresponding to the three damage states increases with the aggravation of the damage state, indicating that an intact structure needs a greater ground motion intensity to transition to a more serious damage state with the same exceedance probability. The corresponding mainshock vulnerability curve can directly show the conditional damage exceedance probability of the bridge structure.

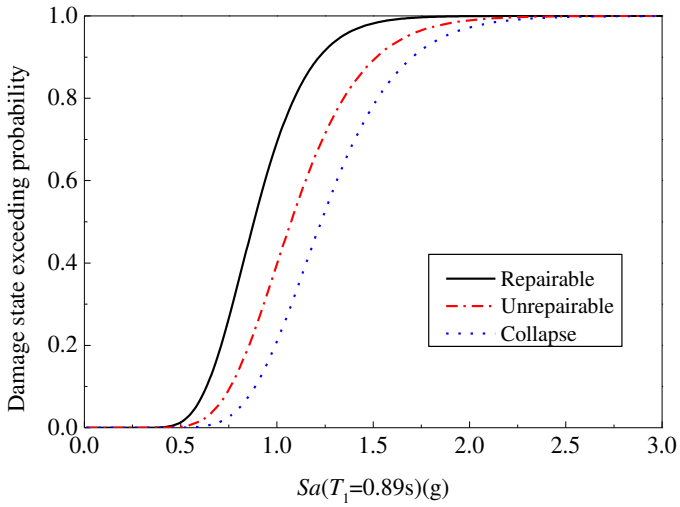

Fig. 6 Mainshock fragility curve for intact bridge

As shown in the figure, the exceedance probability increases with the increase in the abscissa, and gradually approaches from $P(DI_{MS} \geq DI_c) = 0$ to $P(DI_{MS} \geq DI_c) = 1$. This shows that the greater the mainshock intensity, the more prone the structure is to damage transition, and the more dangerous the structure. In addition, the vulnerability curve of the low-damage state is always on the left side of the vulnerability curve corresponding to the high damage state, indicating that an intact structure needs a greater ground motion intensity to transition to a more serious damage state with the same exceedance probability.

3.5 Aftershock fragility analysis

The research object for the aftershock vulnerability is the damaged bridge structure. Compared with an intact bridge structure, it is more likely to suffer further damage when subjected to the same earthquake intensity. Therefore, it is necessary to establish a corresponding aftershock vulnerability model for a damaged structure. The vulnerability function of the damaged structure is assumed to satisfy a lognormal distribution, as shown in Eq. (16).

$$P(LS_{AS} \geq j \mid IM_{AS} = im, DS_{MS} = i) = \Phi\left[\frac{\ln(IM_{AS}) - \ln(\theta_{AS})}{\sigma_{AS}}\right] \tag{16}$$

Here, LS_{AS} represents the final damage state of the bridge structure after the successive actions of the mainshock and aftershock, IM_{AS} represents the aftershock ground motion intensity, and DS_{MS} represents the damage state of the structure after the action of the mainshock. θ_{AS} and σ_{AS} represent the aftershock seismic vulnerability function parameters. The vulnerability model parameters in the formula are calculated based on the EDP criterion method, and the probability of the damaged bridge structure reaching or exceeding the limit state under a specific ground motion is calculated according to Eq. (17).

$$P(DI_{seq} \geq DI_c \mid IM_{AS}, DS_{MS}) = \frac{\sum_{j=1}^{N} F_j}{N} \tag{17}$$

In the above, DI_{seq} denotes the damage index of the bridge subjected to the mainshock and aftershock.

The aftershock vulnerability can be analyzed as follows: a) according to the MSA results of the mainshock, the bridge damage samples are classified into three categories according to their post-mainshock damage state: no damage, repairable damage, and unrepairable damage; b) according to the response results of Double-MSA, the frequency point for the bridge reaching or exceeding a higher damage state under different relative strengths of the mainshock and aftershock are obtained, and c) the statistical parameters of the lognormal distribution function of the seismic vulnerability corresponding to the different transition paths are estimated by the least squares method.

Table 3 Aftershock fragility function parameters

Damage state	Repairable		Unrepairable		Collapse	
	Median	Logarithmic standard deviation	Median	Logarithmic standard deviation	Median	Logarithmic standard deviation
Intact	0.388	0.867	0.742	0.596	0.978	0.573
Repairable	-	-	0.075	2.156	0.423	1.568
Unrepairable	-	-	-	-	0.134	2.198

As it is assumed that the bridge structure can only transition from a lower damage state to a higher damage state, the probabilities corresponding to the transition from the high-damage state to the low-damage state are zero. In the same row, corresponding to the same damage state after the mainshock, the more serious the damage state after the aftershock, the larger the median value of the required ground motion intensity. This shows that the structure needs a higher aftershock intensity to transition from the damage state after the mainshock to the more serious damage state after the aftershock with the same probability. In the same column, with the damage state after the aftershock fixed, the lower the damage state after the mainshock, the larger the median value of the ground motion intensity. This means that it is easier for a more seriously damaged bridge to transition to a highly damaged state. The results show that the median value of the aftershock strength for the repairable structure after the mainshock is 57% less than that for the intact structure after the mainshock, and 86% less than that for an unrepairable structure after the mainshock.

The aftershock vulnerability curves of the damaged bridges are shown in Fig. 7. The three figures correspond to the three different structural damage states after the mainshock. It can be seen that the curve increases monotonously with the increase in the abscissa, and that the

exceedance probability changes from 0 to 1; this reveals that the greater the aftershock intensity, the more likely the structure is to be further damaged.

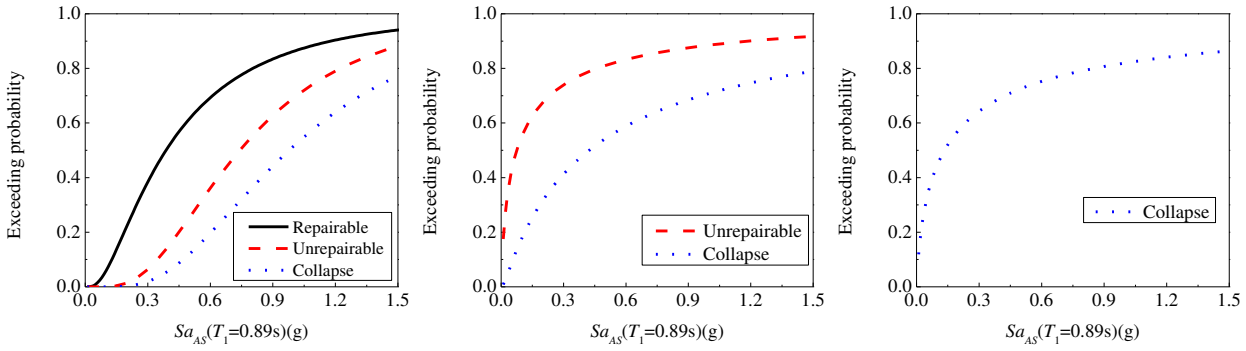

(a) Intact bridge (b) Repairable bridge (c) Unrepairable bridge

Fig. 7 Aftershock fragility curves for bridges in different post-mainshock damage states

When keeping the damage state after the mainshock fixed, the vulnerability curve corresponding to the lower damage state after the aftershock is always on the left side of the vulnerability curve corresponding to the higher damage state after the aftershock. For example, when the exceedance probability is 50%, the aftershock intensities corresponding to the unrepairable damage and collapse damage states are 0.742 g and 0.978 g, respectively, increasing by 31.8%. This means that a damaged structure needs a higher-intensity aftershock to transition with the same exceedance probability. Comparing the three figures, it can be found that when the damage state after the aftershock is fixed, the more serious the damage after the mainshock, the more vulnerable the structure is to damage transition after the aftershock. This verifies that the initial damage after the mainshock has an adverse effect on the structure's further operation.

4 Seismic risk analysis for regular bridge considering the effect of the mainshock-aftershock sequence

4.1 Post-mainshock aftershock seismic risk analysis framework

In this study, multiple aftershocks are considered in the calculation model of the aftershock risk, and damage accumulation is considered in the final damage probability. This study selected 30 days after the main earthquake as the time period for studying the aftershock earthquake risk. According to the assumption that the damage of a structure subjected to an earthquake is only related to the current aftershock intensity and the damage state immediately before this aftershock, and has nothing to do with the damage history (Shokrabadi and Burton 2018; Kumitani and Takada 2009), this study used a non-homogeneous Markov process to simulate the damage of the bridge structure. Therefore, it was necessary to segment the aftershock seismic risk study period with a fixed small time step to ensure that the probability of an aftershock occurring more than once in each small time window could be ignored.

The calculation steps for the aftershock seismic risk are as follows: a) Bayesian updating of the seismicity parameters is conducted to obtain the updated parameters for the seismicity; b) based on the updated parameters and known mainshock information, the aftershock seismic hazard analysis is conducted, and the aftershock intensity exceedance rate function in each time window is obtained; c) the vulnerability curves of the whole bridge structure and the damaged bridge structure are obtained; d) a damage transfer probability matrix is constructed for each time window by convolving the aftershock vulnerability function and the aftershock seismic hazard function of the damaged bridge structure; and e) the probability vector of the initial damage state as determined by the assumed initial damage state after the mainshock is multiplied by the transition probability matrix before the studied time, so as to obtain the time-varying function of the aftershock damage probability corresponding to the initial damage state after different mainshocks.

The convolution in step d is performed according to Eq. (18).

$$\lambda_{i,j}^{s} = \int_{0}^{+\infty} [-(P_{i,j}^{AS}(im) - P_{i,j+1}^{AS}(im))] \mathrm{d}\lambda_{IM,s}^{AS}(im) \tag{18}$$

In the above, s represents the serial number of the time window; $P_{i,j}^{AS}(im)$ represents the conditional damage exceedance probability function; $\lambda_{IM,s}^{AS}(im)$ indicates the aftershock intensity exceedance rate of in the time window s; and the damage transition rate $\lambda_{i,j}^{s}$ is obtained by integrating the product of the conditional damage transition probability and the aftershock intensity exceedance rate on all possible intensities.

Based on the assumption that the damage state transition of the bridge structure satisfies the Poisson model, the probability of one occurrence of a damage state transition can be calculated. The probability of the damage state transition is calculated according to Eq. (19), with the occurrence rate of the damage state transition as the rate of the Poisson distribution.

$$\pi_{i,j}^{s} = \lambda_{i,j}^{s} \exp(-\lambda_{i,j}^{s}) \tag{19}$$

Here, $\pi_{i,j}^{s}$ represents the probability of the damage transition in the time window s. The obtained damage transition probability is placed in the corresponding position of the damage transition matrix according to the subscript to construct the damage transition probability matrix, as shown in Eq. (20).

$$M_s = \begin{bmatrix} \pi_{1,1}^{s} & \mathrm{L} & \pi_{1,m}^{s} \\ \mathrm{M} & \mathrm{O} & \mathrm{M} \\ 0 & \mathrm{L} & \pi_{m,m}^{s} \end{bmatrix} \tag{20}$$

In the above, m represents the total number of damage states, and M_s represents the bridge structure damage transition matrix in the time window s. The damage to a structure without reinforcement or repair is irreversible, and the bridge structure can only transition from a low-damage state to a high-damage state or maintain the original damage state. Therefore, the diagonal

elements and upper triangle position elements of the damage transition matrix are all non-zero values, whereas the lower triangle position elements are all zero. Because the damage state of the structure corresponding to the diagonal elements in each row does not transition, and the damage state transition paths corresponding to other positions in the same row are independent and complementary, the diagonal elements can be calculated directly from the known non-diagonal elements in the same row. According to Eq. (20), the n_s damage transition matrices before the research time t are obtained, and the complex aftershock damage transition matrix M_t^s is obtained using Eq. (21).

$$M_t^s = \prod_{s=1}^{n_s} M_s \tag{21}$$

Here, t represents the research time, and n_s denotes the number of time windows before t. The damage transition matrices in each time window are independent of each other. The structure is not repaired during the seismic risk study period. The complex aftershock damage transition matrix is obtained by multiplying several damage transition matrices in time order.

The goal of step (5) is to obtain the time-varying probability of the bridge structure in each damage state. This can be calculated as follow:

$$d_s = [P_1^{n_s}, P_2^{n_s}, \mathrm{L}\ , P_k^{n_s}, \mathrm{L}\ , P_m^{n_s}] = [P_1^0, P_2^0, \mathrm{L}\ , P_k^0, \mathrm{L}\ , P_m^0] \prod_{s=1}^{n_s} M_s = d_0 M_t^s \tag{22}$$

In the above, P_k^0 represents the probability that the structure is in the k damage state at time zero. In an actual engineering application process, the value is determined according to the actual damage after the mainshock. For example, if the structure is in damage state 2 after the mainshock, the vector is shown as $d_0 = [0,1,0\mathrm{L}\ ,0]_{1\times m}$. $P_k^{n_s}$ represents the probability that the structure is in the k damaged state after the mainshock and subsequent aftershocks.

4.2 Pre-mainshock mainshock-aftershock risk analysis framework

The pre-mainshock mainshock-aftershock risk analysis was performed according to the occurrence of the mainshock. The seismic performance of the bridge structure over its entire life cycle was evaluated by comprehensively considering the impact of the mainshock and aftershocks on the bridge structure at the research site. The impacts of aftershocks occurring within 30 days after the occurrence of the mainshock on the seismic risk of the mainshock and aftershocks were considered in this study. The pre-mainshock mainshock-aftershock risk analysis followed the same logic as the process discussed above for the post-mainshock risk evaluation. In the pre-mainshock mainshock-aftershock risk analysis, the specific information of the future mainshock was unknown, leading to an unknown initial damage state of the bridge structure after the action of the future mainshock. In addition, the prediction model for the aftershock seismic hazard determined that the

possible time, location, and magnitude of the aftershock depended on the specific situation of the triggering mainshock.

In this study, the steps for obtaining the pre-mainshock mainshock-aftershock risk are as follows: a) the generic parameters of the research bridge site provided by the existing literature are used as the seismicity parameters; considering the uncertainty of the mainshock parameters, the mainshock-aftershock seismic hazard analysis is conducted, and the aftershock intensity exceeding the rate function in each time window is obtained; b) the mainshock fragility curves and aftershock fragility curves are obtained; c) in each time window, the damage transition matrix for each time window is obtained by convolving the mainshock-aftershock hazard function with the aftershock vulnerability function; d) the mainshock risk is obtained by convoluting the mainshock vulnerability function and mainshock hazard function, and is expressed by the damage probability vector; e) the annual mean occurrence rate of the mainshock, risk of the mainshock, and damage transition matrices of all time windows are multiplied to obtain the annual mean exceedance rate of each damage state; and f) based on the calculated annual mean occurrence rate, the time-varying damage probability of the mainshock and aftershock in the whole life cycle of the bridge structure is calculated.

The damage state probability in step d can be calculated using Eq. (23).

$$P_j^{MS} = \int_0^{+\infty} (P_{j|IM}^{MS}(im) - P_{j+1|IM}^{MS}(im)) f_{MS}(im)\mathrm{d}im \tag{23}$$

Here, $P_{j|IM}^{MS}(im)$ is the conditional damage exceeding the probability of the bridge structure under the action of the mainshock. $f_{MS}(im)$ represents the probability density function of the mainshock intensity. P_j^{MS} represents the probability that the bridge structure reaches the damage state j under the action of the mainshock, and is obtained according to the integral of the product of the mainshock vulnerability curve and mainshock seismic hazard curve.

$$d_0^{MS} = [P_1^{MS}, P_2^{MS}, \mathrm{L}\ , P_k^{MS}, \mathrm{L}\ , P_m^{MS}] \tag{24}$$

In the above, d_0^{MS} is the probability vector of reaching each damage state of the bridge structure under the action of an unknown mainshock.

The occurrence frequency of the earthquake swarm and mainshock-aftershock damage probability are combined to predict the damage rate of the structure in step (5), as shown in Eq. (25).

$$\lambda^{MSAS} = [\lambda_1^{MSAS}, \lambda_2^{MSAS}, \mathrm{L}\ , \lambda_k^{MSAS}, \mathrm{L}\ , \lambda_m^{MSAS}] = v \cdot d_0^{MS} \prod_{s=1}^{N_s} M_s \tag{25}$$

Here, λ_k^{MSAS} represents the annual mean occurrence rate of the structure reaching the damage state k under the actions of the mainshock and aftershock. v is the annual mean occurrence rate of the mainshock. N_s represents the total number of segmented time windows

during the seismic risk study period.

The annual damage probability in step (6) is calculated based on the assumption that the annual damage of the structure satisfies the homogeneous Poisson model, which has been used by many scholars (Jalayer and Ebrahimian 2017; Trevlopoulos et al. 2020) to represent the time-varying damage of a structure. The homogeneous Poisson model assumes that the structure is damaged to a certain extent after one earthquake swarm (mainshock + multiple aftershocks), but is restored to the initial damage state before the next earthquake swarm. The damage probability of the structure in its life cycle is calculated as follows:

$$P_{LS} = 1 - e^{-\lambda_{LS} T} \tag{26}$$

In the above, P_{LS} represents the damage probability of bridge structure in time window (year) $[0,T]$; T represents the research time of the study, where the maximum value is the life cycle of the bridge structure (100 years); and λ_{LS} represents the annual mean damage rate for all seismic scenarios. In this study, to analyze the influences of aftershock hazards on structural damage, a single mainshock scenario and mainshock-aftershock scenario were considered. The calculation process of the mainshock damage probability was similar to that of the mainshock-aftershock scenario. The annual mean occurrence rate of the mainshock was the same as that of the earthquake swarm. The structure was damaged to a certain extent after one mainshock, but the structure was restored to the damage state before the next mainshock.

4.3 Post-mainshock aftershock seismic risk analysis

In this study, the Wenchuan M_w7.9 earthquake was taken as an example to study the time-varying damage probability of a bridge structure corresponding to three defined damage states within 30 days after the mainshock under the action of the subsequent aftershocks. To satisfy the condition that the probability of more than one aftershock occurrence in each time step could be ignored, this study selected 0.0005 days as the time step, and the probability of more than one aftershock occurring in the time window (day) $[t_0, t_1] = [0, 0.0005]$ as calculated based on the site generic parameters was $P_{AS}(N>1) = 0.015$, which is small. When the step was further reduced, the result of the trial aftershock risk remained unchanged.

Table 4 Damage transition matrix M_1

DS	1	2	3	4
1	9.99E-01	1.03E-03	3.30E-05	1.57E-05
2	0	9.35E-01	5.68E-02	8.11E-03
3	0	0	9.53E-01	4.72E-02
4	0	0	0	1

Table 5 Damage transition matrix M_{60000}

DS	1	2	3	4

1	1	7.28E-07	2.33E-08	1.11E-08
2	0	1	4.26E-05	5.77E-06
3	0	0	1	3.50E-05
4	0	0	0	1

By convolving the aftershock intensity exceeding the rate function and conditional damage probability function in each time window, the damage state transition rate of the structure was obtained. Then, the damage state transition probability and component damage state transition probability matrix were calculated. Taking the first transition probability matrix M_1 and the last transition probability matrix M_{60000} as examples, the results are shown in Tables 4 and 5. It can be seen that the diagonal elements in the same line elements in the table are significantly larger than those in the non-diagonal elements. The longer the time after the mainshock, the more evident this law, indicating a low probability of a bridge structure transition to a high damage state in the aftershock environment. In addition, the diagonal element gradually approaches 1, as a result of the decreasing aftershock hazard with time. With the increase in time, the value of the non-diagonal elements decreases, and the ratio of the non-diagonal elements in M_1 to those in M_{60000} is more than 1000.

The aftershock earthquake risk is shown in Fig. 8. The curves in the figure correspond to different transition paths. After the mainshock, the damaged structure maintains the original damage state or transitions to a highly damaged state with a certain probability. The higher the curve, the greater the transition probability at this time, indicating that the structure is more likely to transition according to this path. In addition, overall, the curve corresponding to each state transition path changes most rapidly at earlier times. This is because the occurrence rate of the aftershock is large just after the occurrence of the mainshock, and the high-frequency aftershocks cause a rapid change in the bridge damage probability. With the decrease in the occurrence rate of the aftershocks, the transition probability varying speed gradually decreases.

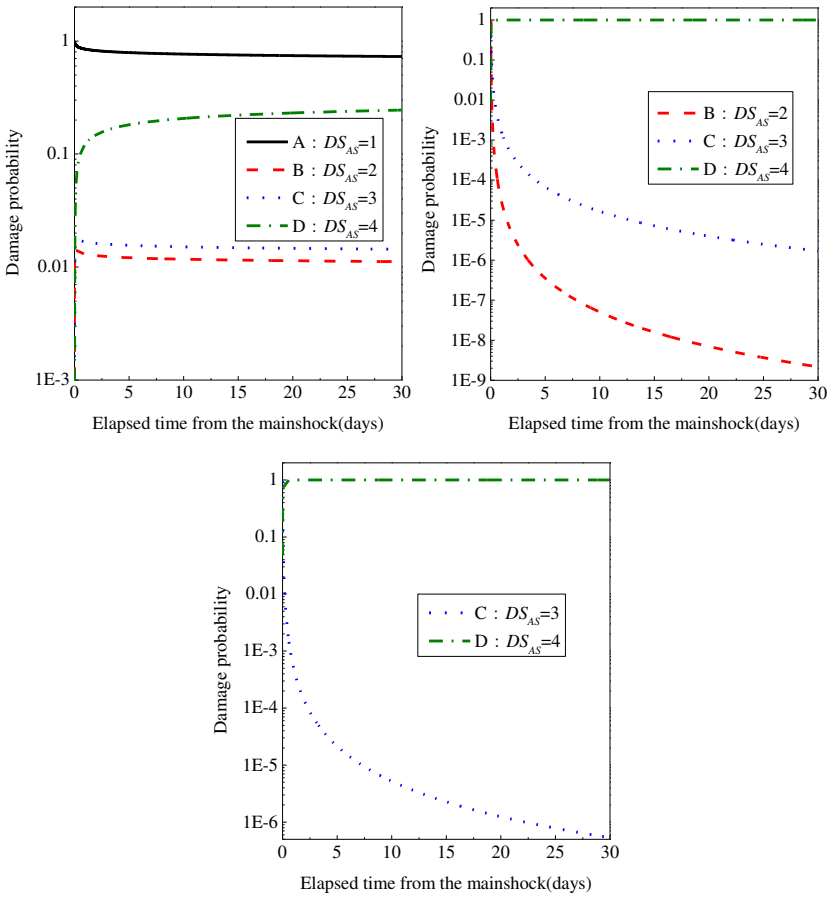

(a) Intact bridge after mainshock (b) Repairable bridge after mainshock (c) Repairable bridge after mainshock

Fig. 8 Damage probability

From observing the curves of the different types of transition paths in the figure, it can be seen that the initial probability value of the bridge remains in the original damage state after the $P(DS_{AS}=i \mid DS_{MS}=i)$ is 1, and decreases with an increase in time. This indicates that in the aftershock environment, the possibility of the bridge structure being in the original state decreases, and the possibility of further damage increases. The more serious the damage state is after the mainshock, the more difficult it is for the structure to remain in its original state.

The collapse probability after the aftershock changes monotonically from the zero point. Immediately after the mainshock, the probability is in a short rapid rise, but the rising speed gradually slows down. It can be seen from the figure that with the aggravation of the damage state after the mainshock, the collapse probability of the bridge structure also increases. The difference in the collapse probability of the structure 30 days after the mainshock is the most evident. The collapse probability corresponding to the intact damage state after the mainshock is 0.245042, the corresponding collapse probability of repairable damage is 0.99998, and the corresponding collapse probability of unrepairable damage is 0.999999. The collapse probability of the structure in the repairable damage state after the mainshock is four times that of the structure in the intact damage state after the mainshock. The collapse probability of the structure in the unrepairable

damage state after the mainshock is greater than that of the former two paths. Because the collapse state is the final damage state, there is no "turn out" path. Therefore, when the damage state after the aftershock is "collapse," regardless of the damage state after the mainshock, the corresponding damage state transfer probability always increases. When the damage state after the mainshock is aggravated, the probability of collapse of the damaged bridge structure is greater. It also shows that the more serious the damage, the more dangerous the bridge structure is in the aftershock environment.

4.4 Pre-mainshock mainshock-aftershock seismic risk analysis

According to the generic parameters of the aftershocks in Wenchuan, the process of the mainshock-aftershock risk analysis in Section 4.2 can be conducted. The annual mean occurrence rate of the Longmenshan Central Fault, with a lower limit of magnitude of 4.0, is 4.76. According to the magnitude-frequency relationship, the annual mean occurrence rate of the lower limit of magnitude 5.0 is 0.89. Finally, the annual mean damage rates of the mainshock and mainshock-aftershock can be obtained, as shown in Table 6. Because the intact structure is not damaged, the mainshock-aftershock probability of reaching an intact damage state is not considered here.

Table 6 Annual mean damage rate for mainshock scenario and mainshock-aftershock scenario ($\times 10^{-6}$)

DS	Repairable	Unrepairable	Collapse
Mainshock scenario	7.34	2.83	2.26
Mainshock-aftershock scenario	8.12	2.85	2.27
Increased percentage	10.63%	0.71%	0.44%

It can be seen from the table that the seismic risk considering the effects of the mainshock and aftershock is greater than that from considering the mainshock only, verifying that aftershocks cannot be ignored in the damage probability prediction. However, the corresponding increase in the percentage of repairable damage is 10.63%, whereas those of unrepairable damage and collapse are 0.71% and 0.44%, respectively. This is because, on the one hand, this bridge is relatively safe, and the bridge structure is not easily seriously damaged at low aftershock hazards. Nevertheless, considering the uncertainty in the magnitude of the mainshock, a large-magnitude mainshock leads to a high aftershock hazard. However, the occurrence probability of such a large-magnitude mainshock is low. While the occurrence probability of a small-magnitude mainshock is high, the triggered aftershock hazard is low. As a result, the mainshock-aftershock hazard is relatively low. The time-varying damage transition probability before the earthquake can be calculated based on Eq. (33), as shown in Fig. 9.

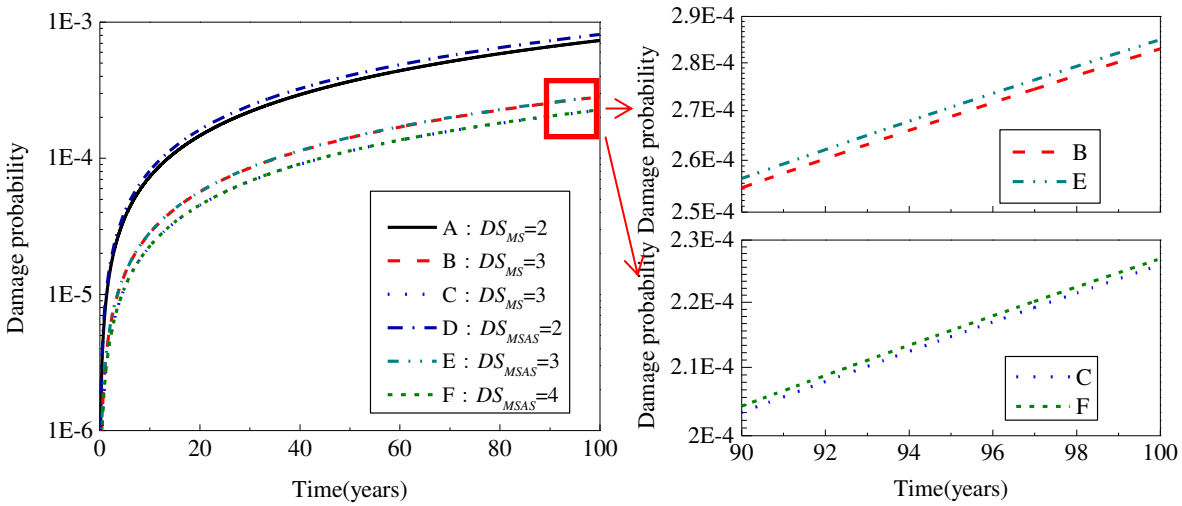

Fig. 9 Damage probability for the bridge in the time window (years) $[0,t]$

As shown in the figure, each curve presents a monotonic increasing law, owing to the irreversibility of the damage state and existence of the seismic hazard. The probability value of each damage state in the figure is low, as a result of a low seismic hazard. However, if three types of damage states are compared, for both the mainshock risk and mainshock-aftershock risk, the probability of being in a repairable damage state is the highest. This indicates that if the bridge analyzed in this study has a state transition, it is easier to reach a repairable damage state in its service life. In addition, the pre-mainshock damage state transition probability curve considering aftershocks is always above the mainshock damage state transition probability curve, indicating that the damage state transition probability considering aftershocks is always greater than that considering only the mainshock. This further verifies the influence of aftershocks on bridge safety, and that bridge damage predictions considering aftershocks are safer.

5 Conclusion

In this study, for a regular girder bridge, an aftershock seismic risk analysis framework and mainshock-aftershock seismic risk framework considering the uncertainty of the mainshock are established. The process involves a mainshock-aftershock seismic hazard analysis and a mainshock-aftershock vulnerability analysis.

Based on a homogeneous Poisson model and the magnitude-frequency relationship, a mainshock hazard analysis model is established. Based on the APSHA model and Bayesian aftershock parameter updating method, a rapid aftershock seismic hazard analysis model is established. Considering the uncertainty regarding the occurrences of the mainshock and aftershock, the seismic hazard analysis model for the mainshock and aftershock is established by combining the PSHA and APSHA. Then, the occurrence rate functions of the ground motion intensity in three earthquake scenarios are produced. It can be found that the occurrence rate of

aftershocks is higher than that of the mainshock just after the mainshock; this indicates the necessity of studying the influence(s) of aftershocks on the structure. In addition, the occurrence rate of aftershocks decreases monotonously with time, and the decrease speed gradually decreases.

Based on the Kunnath damage model, a mainshock vulnerability model and aftershock vulnerability model are established for bridges. Aftershocks can aggravate the structural damage caused by a mainshock, and even lead to collapse. This proves that aftershock effects should not be ignored during earthquake disaster assessments. The mainshock causes structural damage to a certain extent, and the initial damage after the mainshock is not conducive to the bridge structure bearing the aftershock load. When the damage state after the aftershock is fixed, the more serious the initial damage state after the mainshock, the more prone the bridge structure is to a damage state transition under the same aftershock strength, and the bridge structure becomes more dangerous.

The 30-day time-varying damage probability is calculated for a bridge structure subjected to aftershocks occurring after the mainshock, and the influence of the initial damage state on the aftershock risk is verified. It is concluded that in the same aftershock environment, with the aggravation of the initial damage state, the possibility of maintaining the original damage state decreases, whereas the possibility of reaching the collapse state increases. Thus, the initial damage state has an adverse effect on the seismic capacity of the bridge structure.

A mainshock-aftershock seismic risk analysis framework is established, and the annual average damage rate and time-varying damage probability over the entire life cycle of a bridge subjected to a mainshock-aftershock sequence are calculated. Compared with the results of seismic risk analysis under the mainshock alone, the necessity to consider the aftershock effects during seismic damage predictions is verified. It can be observed that the mean annual damage rate of the bridge structure subjected to the mainshock-aftershock sequence is higher than that of the mainshock sequence alone. The value of the damage probability as predicted under the mainshock–aftershock condition is larger over its entire life cycle. This shows that the aftershocks have adverse effects on the safety of the bridge structure, and that a seismic fortification decision based on the damage prediction value for a mainshock-aftershock scenario is relatively safe.

References

Ministry of Transport of the People's Republic of China (2020) 2231-01-2020 J Code for Seismic Design of Highway Bridges.

Alessandri S, Giannini R, Paolacci F (2013) Aftershock risk assessment and the decision to open traffic on bridges. Earthq Eng Struct Dyn 42:2255–75. https://doi.org/10.1002/eqe.2324.

Boore DM, Atkinson GM (2008) Ground-motion prediction equations for the average horizontal component of PGA, PGV, and 5%-damped PSA at spectral periods between 0.01 s and 10.0 s. Earthq Spectra 24:99–138. https://doi.org/10.1193/1.2830434.

Boyd OS (2012) Including Foreshocks and Aftershocks in Time-Independent Probabilistic Seismic-Hazard Analyses. Bull Seismol Soc Am 102:909–17. https://doi.org/10.1785/0120110008.

Chadwell CB, Imbsen RA (200$) XTRACT: A tool for axial force - Ultimate curvature interactions. Proc. 2004 Struct. Congr. - Build Past Secur Futur p. 1–9. https://doi.org/10.1061/40700(2004)178.

Ebrahimian H, Jalayer F, Asprone D, Lombardi AM, Marzocchi W, Prota A (2014) Adaptive Daily Forecasting of Seismic Aftershock Hazard. Bull Seismol Soc Am 104:145–61. https://doi.org/10.1785/0120130040.

Ebrahimian H, Jalayer F, Asprone D, Lombardi AM, Marzocchi W, Prota A, et al. (2014) A performance-based framework for adaptive seismic aftershock risk assessment. Earthq Eng Struct Dyn 43:2179–97. https://doi.org/10.1002/eqe.2444.

Fu JC (2015) Study on seismic vulnerability of bridge subjected to mainshock-aftershock sequences. Fuzhou University.

García D, Wald DJ, Hearne MG (2012) A global earthquake discrimination scheme to optimize ground-motion prediction equation selection. Bull Seismol Soc Am 102:185–203. https://doi.org/10.1785/0120110124.

Gutenberg, Beno and Richter CF (1944) Frequency of earthquakes in California. Bull Seismol Soc Am 34:185–8. https://doi.org/10.1785/BSSA0340040185.

Iervolino I, Giorgio M, Polidoro B (2014) Sequence-based probabilistic seismic hazard analysis. Bull Seismol Soc Am 104: 1006–12. https://doi.org/10.1785/0120130207.

Jalayer F, Ebrahimian H (2017) Seismic risk assessment considering cumulative damage due to aftershocks. Earthq Eng Struct Dyn 46:369–89. https://doi.org/10.1002/eqe.2792.

Kiureghian A Der, Ang A (1977) A fault-rupture model for seismic risk analysis. Bull Seismol Soc Am 67:1173–94.

Kumar S, Usami T (1996) Damage Evaluation in Steel Box Columns by Cyclic Loading Tests. J Struct Eng 122:626–34. https://doi.org/10.1061/(asce)0733-9445(1996)122:6(626).

Kumitani S, Takada T (2009) Probabilistic assessment of buildings damage considering aftershocks of earthquakes. J Struct Constr Eng 74:459–65. https://doi.org/10.3130/aijs.74.459.

Kunnath, Sashi K and Reinhorn, Andrei M and Park YJ (1990) Analytical modeling of inelastic seismic response of R/C structures. J Struct Eng 116:996–1017.

Mazzoni S., McKenna F., Scott MH, Fenves GL (2006) OpenSees Command Language Manual. Pacific Earthq Eng Res Cent 264:137–58.

Michael AJ, McBride SK, Hardebeck JL, Barall M, Martinez E, Page MT, et al (2019) Statistical seismology and communication of the USGS operational aftershock forecasts for the 30 November 2018 Mw 7.1 Anchorage, Alaska, earthquake. Seismol Res Lett 91:153–73. https://doi.org/10.1785/0220190196.

Moehle J and Deierlein GG (2004) A framework methodology for performance-based earthquake engineering. 13th World Conf. Earthq. Eng., Vancouver, Canada, p. 679.

Ogata Y (1983) Estimation of the parameters in the modified omori formula for aftershock frequencies by the maximum likelihood procedure. J Phys Earth 31:115–24. https://doi.org/10.4294/jpe1952.31.115.

Page MT, van Der Elst N, Hardebeck J, Felzer K, Michael AJ (2016) Three ingredients for improved global aftershock forecasts: Tectonic region, time-dependent catalog incompleteness, and intersequence variability. Bull Seismol Soc Am 106:2290–301. https://doi.org/10.1785/0120160073.

Park Y, Ang AH-S (1985) Mechanistic Seismic Damage Model for Reinforced Concrete. J Struct Eng 111:722–39. https://doi.org/10.1061/(asce)0733-9445(1985)111:4(722).

Reasenberg PA, Jones LM (1989) Earthquake Hazard After a Mainshock in California. Science (80-) 243:1173–6. https://doi.org/10.1126/science.243.4895.1173.

Ryu H, Luco N, Uma SR, Liel AB (2011) Developing fragilities for mainshock-damaged structures through incremental dynamic analysis. Ninth Pacific Conf. Earthq. Eng., Auckland, New Zeal.

Shokrabadi M, Burton HV (2018) Risk-based assessment of aftershock and mainshock-aftershock seismic performance of reinforced concrete frames. Struct Saf 73:64–74. https://doi.org/10.1016/j.strusafe.2018.03.003.

Stone, WC and Taylor AW. Seismic performance of circular bridge columns designed in accordance with AASHTO/CALTRANS standards 1993.

Toro GR, Silva WJ (2001) Scenario Earthquakes for Saint Louis, MO, and Memphis, TN, and Seismic Hazard Maps for the CEUS Region Including the Effect of Site Condition. Technical Report.

Trevlopoulos K, Guéguen P, Helmstetter A, Cotton F (2020) Earthquake risk in reinforced concrete buildings during aftershock sequences based on period elongation and operational earthquake forecasting. Struct Saf 84:101922. https://doi.org/10.1016/j.strusafe.2020.101922.

Utsu T, Ogata Y (1995)The centenary of the omori formula for a decay law of aftershock activity. J Phys Earth 43:1–33. https://doi.org/10.4294/jpe1952.43.1.

Veismoradi S, Cheraghi A, Darvishan E (2018) Probabilistic mainshock-aftershock collapse risk assessment of buckling restrained braced frames. Soil Dyn Earthq Eng 115:205–16.

https://doi.org/10.1016/j.soildyn.2018.08.029.

Wells DL, Coppersmith KJ (1994) New empirical relationships among magnitude, rupture length, rupture width, rupture area, and surface displacement. Bull - Seismol Soc Am 84:974–1002.

Wen W, Zhai C, Ji D, Li S, Xie L (2017) Framework for the vulnerability assessment of structure under mainshock-aftershock sequences. Soil Dyn Earthq Eng 101:41–52. https://doi.org/10.1016/j.soildyn.2017.07.002.

Ye A J, Hu S D FLC (2001) Simulation analysis of seismic performance of bridge bearings. J Tongji Univ 29:6–9.

Yeo GL, Cornell CA (2009) A probabilistic framework for quantification of aftershock ground-motion hazard in California: Methodology and parametric study. Earthq Eng Struct Dyn 38:45–60. https://doi.org/10.1002/eqe.840.

Zhang L, Goda K, De Luca F, De Risi R (2020) Mainshock-aftershock state-dependent fragility curves: A case of wood-frame houses in British Columbia, Canada. Earthq Eng Struct Dyn 49:884–903. https://doi.org/10.1002/eqe.3269.

Statements and Declarations

Funding

The research reported in this publication was supported by the Natural Science Foundation of Fujian Province (2020J01478).

Competing Interests

The authors declare that they have no known competing financial interests or personal relationships that could have appeared to influence the work reported in this paper.